Journal of the Association for Research in Otolaryngology (2024) 25:575–589
https://doi.org/10.1007/s10162-024-00968-9

ORIGINAL ARTICLE: GENERAL RESEARCH

Evaluating the Correlation Between Stimulus Frequency Otoacoustic Emission Group Delays and Tuning Sharpness in a Cochlear Model

Yiwei Xia[1,2] · **George Samaras**[1,2] · **Julien Meaud**[1,2,3]

Received: 11 July 2024 / Accepted: 27 October 2024 / Published online: 7 November 2024

Abstract

Purpose: A theoretical framework based on coherent reflection and filter theory predicts that the phase-gradient delays of stimulus frequency otoacoustic emissions (SFOAEs) are correlated with tuning sharpness in the mammalian cochlea. In this paper, we use a computational model of the cochlea to test this theory and to evaluate how SFOAE phase-gradient delays may be used to estimate the sharpness of cochlear tuning. **Methods:** This study is based on a physiologically motivated model which has been previously shown to predict key aspects of cochlear micromechanics. Cochlear roughness is introduced to model the reflection mechanism which underlies SFOAE generation. We then examine how varying the values of key model parameters or of the sound pressure level of the stimulus affects the relation between cochlear tuning and SFOAE delays. Finally, we quantify the ability of model simulations of SFOAE phase-gradient delays to provide reliable estimates of the tuning sharpness of the model. **Results:** We find that variations of model parameters that cause significant broadening of basilar membrane (BM) tuning typically give rise to a sizeable reduction in SFOAE phase-gradient delays. However, some changes in model parameters may cause a significant broadening of BM tuning with only a moderate decrease in SFOAE delays. SFOAE delays can be used to estimate the tuning sharpness of the model with reasonable accuracy only in cases where broadening of cochlear tuning is associated with a significant reduction in SFOAE delays. **Conclusion:** The numerical results provide key insights about the correlations between cochlear tuning and SFOAE delays.

Keywords Otoacoustic emissions · Cochlear tuning · Cochlear model · Group delay

Introduction

The mammalian cochlea is a sensory system known for its sharp frequency selectivity, high sensitivity, and broad dynamic range [1]. These characteristics arise due to an active nonlinear feedback mechanism, called the cochlear amplifier, which is linked to the electromechanical response of outer hair cells (OHCs). This feedback mechanism is also responsible for the generation of sounds by the cochlea, which are called otoacoustic emissions (OAEs). OAEs are commonly measured in the ear canal (EC) to provide a simple, efficient, and noninvasive measure of cochlear function in both research and clinical practice [2]. Some OAEs are emitted due to a linear reflection mechanism caused by impedance perturbations in the cochlear partition according to coherent reflection theory [3, 4]. This includes stimulus frequency OAEs (SFOAEs), which are sounds emitted by the cochlea at the frequency of the external stimulus and are the focus of the current study. One of the key characteristics of reflection OAEs, including SFOAEs [4], is a rapidly rotating phase. The phase gradient of SFOAEs characterizes the latency of the emissions and is associated with the frequency selectivity and sharpness of tuning of the mammalian cochlea. This link between SFOAE phase-gradient delay and tuning sharpness can be explained by a theoretical framework that combines the theory of coherent reflection and filter theory [5].

The theory of coherent reflection predicts that the normalized SFOAE phase-gradient delay (expressed in number

Yiwei Xia and George Samaras contributed equally to this work

✉ Julien Meaud
julien.meaud@me.gatech.edu

[1] George W. Woodruff School of Mechanical Engineering Atlanta, GA Atlanta 30332, USA

[2] Georgia Institute of Technology, 771 Ferst Drive, Atlanta 30332, GA, USA

[3] Petit Institute for Bioengineering and Bioscience, Georgia Institute of Technology, North Avenue, Atlanta 30332, GA, USA

of periods), N_{SFOAE}, is linked to the normalized phase-gradient delay of the BM at the best place (BP), N_{BM}. More specifically, the ratio of N_{SFOAE} to the phase-gradient delay of the pressure difference waves at BP is expected to be two since SFOAE requires round-trip wave propagation; however, the ratio of N_{SFOAE} to the BM group delay at BP, N_{BM}, is predicted to be a bit less than two due to the difference between the group delays of the BM response and fluid pressure [5]. Filter theory predicts the relation between N_{BM} and the sharpness of tuning of the BM (which can be evaluated using the equivalent rectangular bandwidth quality factor, Q_{ERB}). If the type and order of cochlear filters are assumed to be the same across longitudinal locations and across species, the relation between N_{BM} and Q_{ERB} is expected to remain invariant. Combined with the theory of coherent reflection, this theoretical framework implies that the SFOAE tuning ratio (defined as the ratio of Q_{ERB} to N_{SFOAE}) is invariant across locations and species. Experiments have shown that the tuning ratio is indeed approximately invariant among cats, guinea pigs, and chinchillas, at least for characteristic frequencies (CFs) above the apical-basal transition [5]. This opened the possibility of determining cochlear tuning from SFOAE phase-gradient delay [5]. Using the SFOAE group delay to estimate cochlear tuning in humans led to the conclusion that human ears are more sharply tuned than those of other species [5]. However, the theoretical framework underlying the estimation of cochlear tuning from SFOAE delays (coherent reflection theory and filter theory) relies on a series of assumptions and approximations. One of the key assumptions is that the type and order of cochlear filters are invariant; another one is that the ratio of SFOAE delays to BM delays is invariant.

In this work, we aim to test this theoretical framework using our previously developed cochlear model. After comparing the BM and SFOAE responses of the model to available experimental data in gerbils, we study how changes in cochlear tuning are correlated with changes in SFOAE phase-gradient delays. To vary the sharpness of cochlear tuning and SFOAE delays, the values of key model parameters or the stimulus level are varied. We then examine whether the simulated values for N_{SFOAE} can be used to estimate the sharpness of cochlear tuning in the model. Analysis of the numerical results gives new insights about the link between SFOAE delays and cochlear tuning.

Methods

Cochlear Model

This work is based on a three-dimensional (3D) model of the gerbil cochlea. This model, which couples mechanical, electrical, and acoustical domains, has been described in detail in previous works [6, 7]. The micromechanical model of the organ of Corti (OoC) includes one degree of freedom (DOF) for the BM and two DOFs for the TM (shear and bending) at each longitudinal cross-section. Within each cross-section, elastic springs represent the elasticity of the BM, TM attachment to the spiral limbus, reticular lamina (RL), OHC main body, and hair bundle (HB) [8]. Furthermore, these cross-sections are directly coupled to each other via structural longitudinal coupling, which is considered in the BM and TM, as described in Ref. [9].

The micromechanical model and the electrical model are coupled to each other due to mechano-electrical transduction (MET) and somatic electromotility. The MET current is a nonlinear function of the angular deflection of the OHC HB relative to the reticular lamina, $\theta_{hb/rl}$:

$$i_{MET}(\theta_{hb/rl}) = I_{hb}^{max} \times \left[\frac{1}{1+\exp(-\frac{L_{hb}\theta_{hb/rl}-X_0}{\Delta X})} - P_0^s\right], \tag{1}$$

where L_{hb} is the length of the HB; X_0 and ΔX are constant values; P_0^s is the resting open probability of the HB MET channel; and I_{hb} is the saturating MET current and is given by $I_{hb}^{max} = G_{hb}^{max}\Delta V_{hb}^0$ where G_{hb}^{max} is the saturating MET conductance and ΔV_{hb}^0 is the resting value of the difference between the scala media potential and the intracellular OHC potential. Somatic electromotility is modeled using linear reciprocal equations:

$$i_{som} = -\epsilon_3 \dot{u}_{ohc}^{comp} \tag{2}$$

$$f_{ohc} = \epsilon_3 \Delta V_{ohc}, \tag{3}$$

where ϵ_3 is the electromechanical coupling coefficient. Equation 2 relates the OHC compression rate $\dot{u}_{ohc}^{comp}$ to the somatic current i_{som}. Equation 3 relates the OHC transmembrane potential (ΔV_{ohc}, defined as the difference between the intracellular OHC potential and the scala tympani potential) and the force applied by the OHCs on the BM and RL in the extension direction, f_{ohc}.

All results except for the study of the effect of sound pressure level were obtained using a linear frequency-domain implementation of the model. The study of the effect of sound pressure level is based on a nonlinear time-domain implementation of the model. The use of a linear frequency-domain model is advantageous as this model runs much faster than the nonlinear time-domain model. The nonlinear model converges to the linear model at low stimulus levels (20 dB SPL and below).

Except for the parameters listed in the table in Table 1, all parameter values for the baseline model are identical to the values used in our previous paper [7]. The smooth version of the cochlear model (i.e., the version of the model without cochlear roughness, which is introduced in the next subsection) has been calibrated based on previously published in

vivo BM measurements in gerbils at four different locations: the 18 kHz [10] (Fig. 1 A and F), 26 kHz [11] (Fig. 1 B and G), 35.5 kHz [12] (Fig. 1 C and H), and 45.5 kHz [13] (Fig. 1 D and I) characteristic places (CPs). The values of model parameters were chosen such that the active to passive gain of the model is similar to that observed experimentally; however, the model gain is a few dB higher than experiments, especially at the 26 kHz CP. Appendix 2 shows the responses of a model with reduced MET current and illustrates how reducing MET conductance to bring the gain closer to that observed experimentally has little effect on the relationships between tuning sharpness and group delays.

The equivalent rectangular bandwidth (ERB) of the smooth model BM response was used to calculate the quality factor, Q_{ERB}:

$$Q_{ERB}(f_{\mathrm{CF}}) = f_{\mathrm{CF}}/\mathrm{ERB}(f_{\mathrm{CF}}) \tag{4}$$

where ERB is the equivalent rectangular bandwidth at the local characteristic frequency, f_{CF} [14]. Note that the characteristic frequency (CF) and best frequency (BF) both refer to the frequency of maximum BM response at a fixed longitudinal location: CF corresponds to the frequency of the maximum response for low-level stimuli, whereas BF refers to the level-dependent frequency of maximum response [15]. Similarly, the CP is the location of maximum response for low-level stimuli of a given frequency, whereas the BP is the level-dependent location of maximum response. Q_{ERB} is predicted to increase as CF increases (Fig. 1E), in a manner similar to in vivo measurements in gerbil from Ref. [16]. However, the predicted phase has a steeper slope than experiments around the CF (Fig. 1 F–I), implying that the model overpredicts the BM group delay at CF. The normalized group delay at CF expressed in number of cycles, N_{BM}, is plotted as a function of CF in Fig. 1J. The simulated N_{BM} increases as CF increases, as observed in the experimental results in the gerbil cochlea reported by Charaziak and Shera [16]. However, the slope of the N_{BM} vs. CF curve is shallower than in the experiments; furthermore, the simulated N_{BM} values are higher than the experimental values by a factor of 1.5 to 2.5. The simulated N_{BM} values are also above the experimental values in the model with reduced MET current shown in Appendix 2.

Cochlear Roughness and SFOAE Simulations

In order to simulate reflection OAEs, cochlear roughness is introduced in the BM stiffness. In the model with cochlear roughness, the BM stiffness of the smooth model, $K_{bm}(x)|_{smooth}$, is perturbed according to the equation:

$$K_{bm}(x)|_{rough} = \Big(1 + \sigma_R r(x)\Big)\, K_{bm}(x)|_{smooth} \tag{5}$$

where $r(x)$ is a number generated by a random number generation based on a normal distribution with a standard deviation of one, and σ_R is the standard deviation of the perturbations from the smooth case. $\sigma_R = 0.1\%$ has been used throughout this work for the rough models as this value results in similar

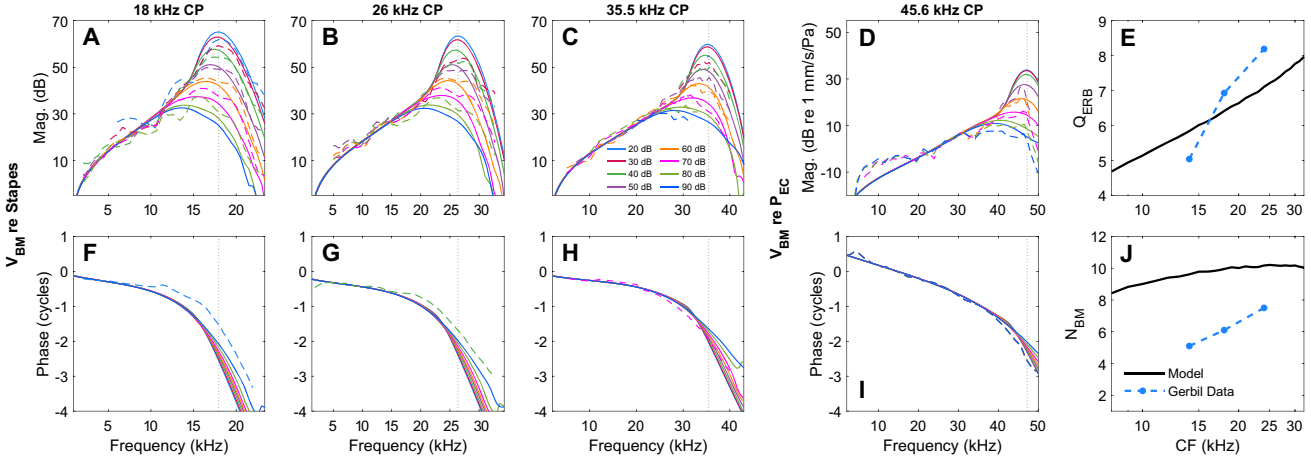

Fig. 1 Comparison of the pure tone responses predicted by the nonlinear model to in vivo experiments in gerbil. **A**–**C** and **F**–**H** The amplitude and phase of the BM velocity relative to the stapes velocity; **D** and **I** the amplitude and phase of the BM velocity relative to the EC pressure. For the amplitude, experimental curves were shifted vertically so that they overlap with the model in the low-frequency tail of the curves. Simulations (solid lines) are compared to measurements (dashed lines) in individual animals at 18 kHz CP from He and Ren [10] in **A** and **F**; at the 26 kHz CP from He and Ren [11] in **B** and **G**; at the 35.5 kHz CP from Overstreet et al. [12] in **C** and **H**; and at the 45.5 kHz CP from Cho et al. [13] in **D** and **I**. Model SPLs are from 20 to 90 dB in 10 dB steps. Experimental SPLs are from 20 to 80 dB in **A**, 30 to 80 dB in **B**, and 20 to 90 dB in **C**, all in 10 dB steps. In **D**, experimental SPLs are 58, 66, 78, 86, and 92 dB. The experimentally measured phases in **F**–**I** are plotted at a single stimulus level (20 dB SPL; 30 dB SPL in **G**; 70 dB SPL in **H**; 58 dB SPL in **I**). **E** Q_{ERB} of the BM velocity at low SPL. **J** Normalized group delay, (N_{BM}) of the BM at the CP at low SPL. Simulations in **E** and **J** are compared to experimental measurements in gerbils (average of data for $n = 16$ animals) from Charaziak and Shera [16]

SFOAE levels and fine structure as in experiments in gerbils [16]. A random number seed (RNS) is used in the model to initialize the random number generator, which enables the possibility of simulating a family of various roughness profiles by using different RNS values. Simulations with different RNS values mimic the measurement of OAEs in multiple cochleae.

Calculation of the SFOAE is based on the reflection component in the EC pressure, which is the vector difference between the steady-state pure tone response of the models with and without roughness (smooth model). This method, which is advantageous because it can be applied to linear frequency-domain simulations, differs from the nonlinear compression and suppression methods, which are typically used in experiments. We showed in Ref. [17] that the method used in the current paper yields SFOAE amplitudes and phases that are nearly identical to those obtained using the nonlinear compression method. Vencovsky et al. [18] have also shown using their nonlinear cochlear model that the method currently used here yields nearly identical results to the nonlinear compression method and suppression method at least for frequencies above 0.9 kHz; however, short latency components may be present when the compression or suppression methods are used. The short latency components present when the compression method or the suppression method is applied would not affect the key results of this paper as they would be filtered out by the method introduced in the next section.

Robust Calculation of SFOAE Group Delays

SFOAEs are the summation of multiple components of different delays, which include a short latency component and components of longer latency corresponding to multiple internal reflections [19]. Interference between these multiple components can complicate the interpretation of SFOAEs and introduce bias (overestimation) in obtaining the phase-gradient delays. The link between BM tuning and SFOAE phase-gradient delay is expected to be strong only if the first reflection component is considered. To determine the first reflection component, the following method, illustrated in Fig. 2, is applied. The SFOAEs as a function of frequency (shown in Fig. 2 A and C) are first converted to the time-domain by applying an inverse fast Fourier transform (IFFT) (the black line in Fig. 2B) and are then transformed into time-frequency representations by using continuous wavelet transform (CWT) (Fig. 2D), in a similar manner to the method proposed by Moleti et al. [20]. The CWT provides the constituent time-varying spectral components of the SFOAE. To identify the 1st reflection component, the group delay of the BM predicted by the smooth model at the frequency-dependent best place, $\tau_{BM}(x)$, is first calculated. Time-frequency filtering is applied over the CWT to identify the short latency (delays less than $1\times\tau_{BM}$), 1st reflection (delays between $1\times$ and $3\times\tau_{BM}$) and 2nd reflection (delays between $3\times$ and $5\times\tau_{BM}$) components. These components can be visualized in the time domain (red, gold, and blue lines in Fig. 2B). After applying a fast Fourier transform, the amplitude and phase of the 1st and 2nd reflection components are obtained in the frequency domain (Fig. 2 A and C).

The peak-picking algorithm is then implemented [19]. This method only considers the values of the group delay near frequencies corresponding to peaks in the SFOAE level of the 1st reflection component. Here, the peak-picking selection includes the peak itself and one point on either side of the peak (Fig. 2A). To obtain the curve of phase-gradient delay of SFOAE vs. frequency, the time-frequency filtering and peak-picking method was applied to simulations obtained with multiple RNS (64 RNS values for linear simulations; 16 RNS values for nonlinear simulations), before applying loess smoothing [19] using a span of 50% to establish the general trend for the group delay vs. frequency curve (e.g., Fig. 3C).

Variations in the Model Parameters and in the Stimulus Level

Three model parameters were varied from their baseline values used in the calibrated model to study how changes in cochlear tuning are correlated with changes in SFOAE group delays. For all these variations, the state-space formulation of the model allows us to check the linear stability of each case before running the frequency-domain simulations [21, 22], which is important because a linear frequency-domain simulation would not be meaningful in case of a model with a linear instability (i.e., a model that predicts the generation of a spontaneous OAE). For each parameter, the variation was parameterized using a non-dimensional scaling factor, defined such that a value of one corresponds to the baseline, fully active, and calibrated model shown in Fig. 1.

The first parameter is the saturating MET current, I_{hb}^{max}, which was parameterized using the non-dimensional scaling factor SF_{MET}. $SF_{\mathrm{MET}} = 0$ corresponds to a passive model; a value between 1 and 0 corresponds to partial loss of OHC function (either due to a reduction in the MET channel saturating conductance G_{hb}^{max} or to reduction in ΔV_{hb}^{0} linked to a reduction in the endocochlear potential, which is one possible source of age-related hearing loss [23]). In this study, SF_{MET} is varied between 1 and 0.44.

The second parameter is the TM longitudinal coupling scaling factor (SF_{TMLC}), which scales the values of longitudinal stiffness and viscosity of the TM [9] from their baseline values [6]. Experimental studies, which have examined how genetic mutations that affect the TM proteins alter TM properties and cochlear function in some transgenic mice [24–26], and the

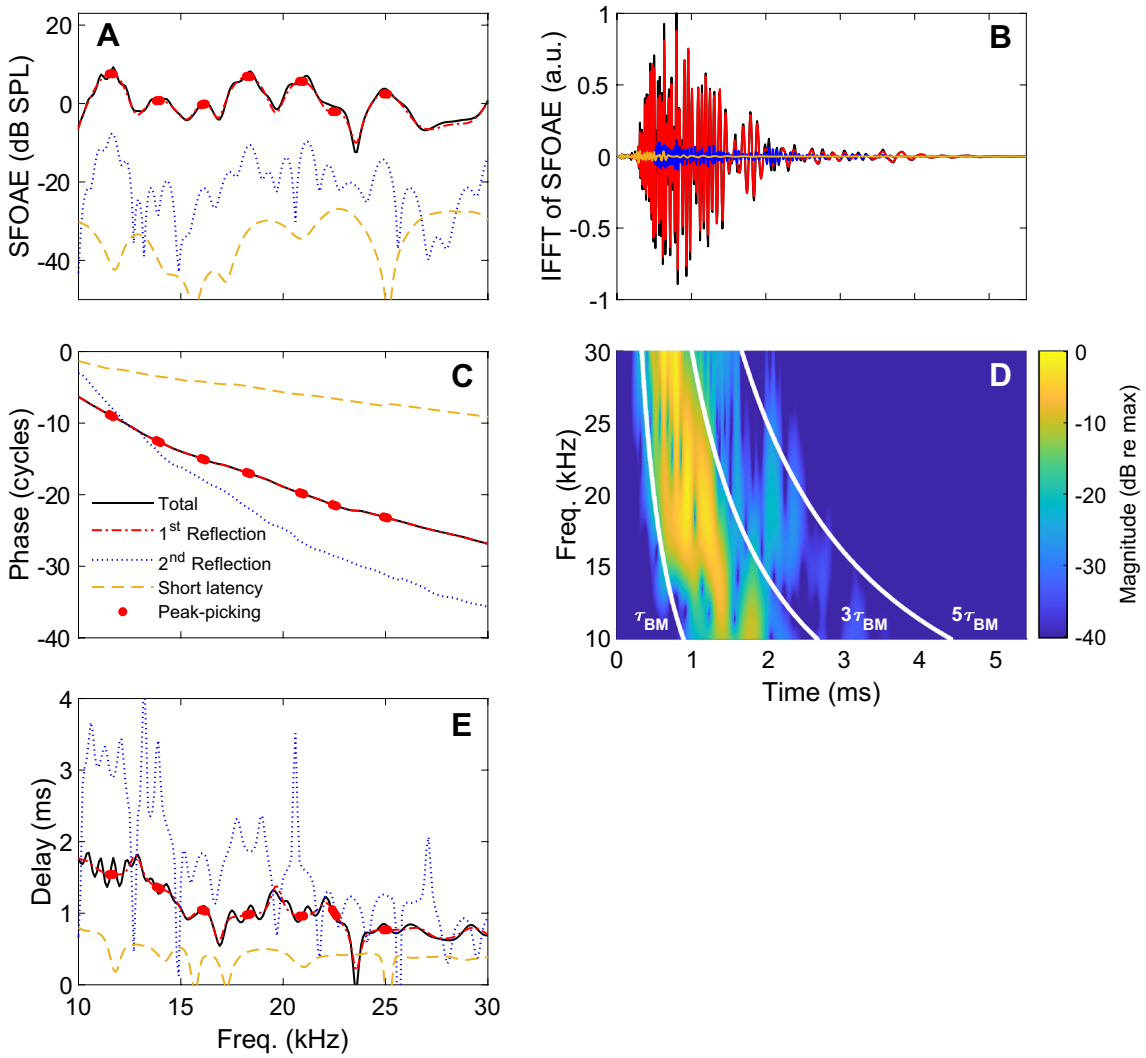

Fig. 2 Illustration of applying time-frequency filtering and of the peak-picking method. Amplitude (**A**) and phase (**C**) of SFOAE predicted by the baseline linear cochlear model with roughness (with RNS = 0). **B** Inverse fast Fourier transform of the SFOAE response. **D** Time-frequency distribution of SFOAE response by using continuous wavelet transform (CWT). White curves indicate 1, 3, and 5 times the phase-gradient delay of BM responses at CF; these curves are used as guidelines to filter the SFOAE responses into short latency, and 1st and 2nd reflection components. **E** SFOAE phase-gradient delay, τ_{SFOAE}. In **A**–**C** and **E**, the black, red, blue, and gold lines represent the total SFOAE response (i.e., unfiltered response), the first reflection component, the second reflection component, and the short latency component, respectively; the red dots correspond to the frequencies of the peaks of the 1st reflection component and to the frequencies just below and just above the peaks. The SFOAE delays are evaluated at the frequencies identified by the peak-picking method

theoretical results from Ref. [9], which showed that TM longitudinal coupling tends to broaden cochlear tuning, motivate us to study the effect of SF_{TMLC} on SFOAE delays. In the current study, longitudinal coupling was increased by varying SF_{TMLC} between 1 and 8 in order to broaden cochlear tuning.

The third model parameter that has been varied is the OoC impedance scaling factor (SF_{OoC}). SF_{OoC} scales the stiffness of OHCs, RL, and hair bundles (HBs), as well as the bending stiffness, mass, and damping of TM from the corresponding baseline values. This variation is motivated by our recent results which showed that the impedance of OoC components affects the tuning of the BM vibrations [7]. SF_{OoC} was varied between 1 and 0.4.

In addition to these three parameter variations, a nonlinear implementation of the baseline model was run at stimulus levels from 0 to 60 dB SPL to evaluate how an increase in SPL affects the link between cochlear tuning and SFOAE delays.

Results

SFOAE Predictions of the Baseline Cochlear Model

Figure 3A and B shows the amplitude and phase of the SFOAEs predicted by the baseline cochlear model with roughness

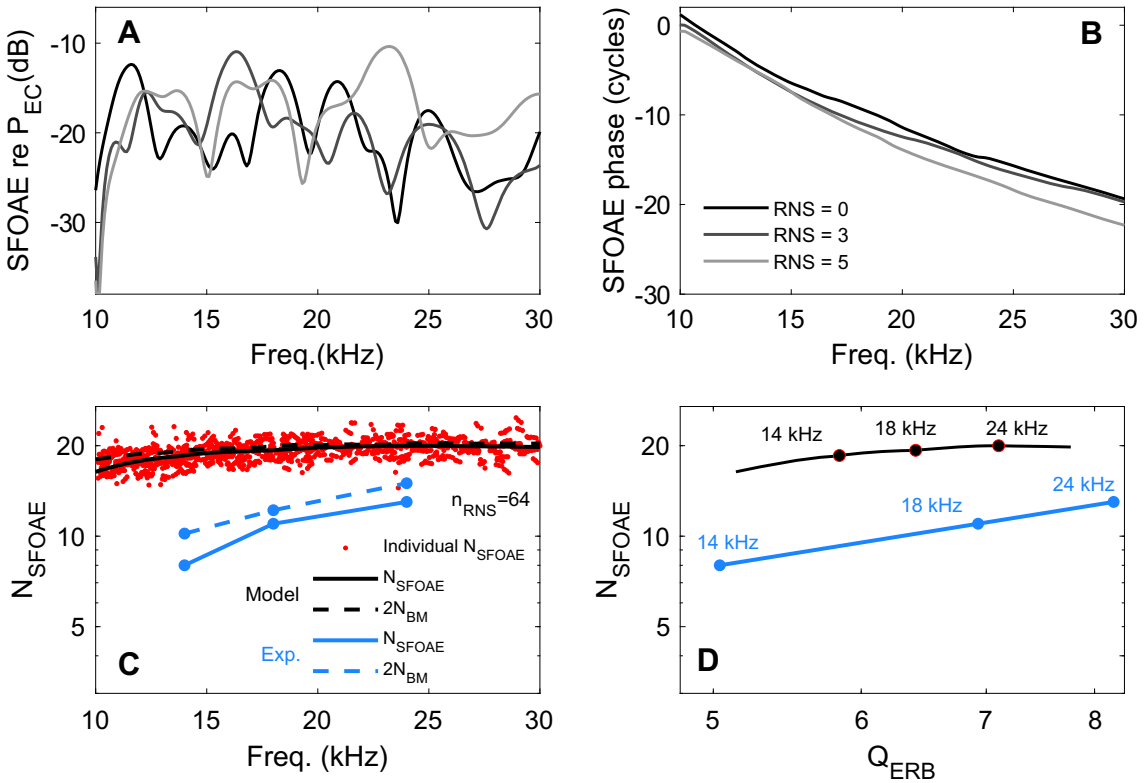

Fig. 3 Model overview of SFOAE characteristics in response to a 20 dB SPL stimulus. Amplitude (**A**) and phase (**B**) of the 1st reflection component of the SFOAE predicted for 3 different RNS values. **C** N_{SFOAE} plotted vs. frequency. Dots in **C** show N_{SFOAE} for 64 RNS, where each point is calculated at the frequency of the peak-picking method applied to the 1st reflection component of the SFOAE. The solid line is a loess fit of the points using a span of 50%. The dashed line corresponds to $2 \times N_{BM}$. D. N_{SFOAE} plotted vs. Q_{ERB}. In **C**, the experimental data (average of $n = 5$ animals) are from Charaziak and Shera [16]. In **D**, the blue line is the following empirical equation from Charaziak and Shera [16]: $N_{SFOAE} = Q_{ERB}/0.63$ where Q_{ERB} corresponds to the quality factor of the BM

for three different RNS values, which mimic measurements in different cochleae. For each RNS, the amplitude has many peaks and valleys, i.e., fine structure, which depend on the RNS value. The predicted SFOAE has approximately the same level as observed in gerbils in response to low-level stimuli [16]; however, the model predictions seem to lack the broad macrostructure observed in these experiments, where SFOAE drops to a low level over a relatively broad frequency range. The SFOAE phase has a steep slope and accumulates about 25–30 cycles from 10 to 30 kHz. The SFOAE phase-gradient delay was calculated based on the procedure described in the methods, i.e., time-frequency filtering was applied to isolate the 1st reflection component before applying the peak-picking method. Throughout the results, the phase-gradient delay, N_{SFOAE} was expressed in number of cycles:

$$N_{SFOAE} = -\frac{f}{2\pi}\frac{d\angle P_{SFOAE}}{df} \tag{6}$$

where $\angle P_{SFOAE}$ refers to the phase of the SFOAE expressed in radians and f is the frequency in Hz. The phase-gradient delays at the peak-picked frequencies are aggregated using simulations of all 64 RNS values using a loess fit and plotted as the normalized phase-gradient delay (red dots in Fig. 3C). The loess fit of the N_{SFOAE} predicted for all RNS values generally increases as frequency increases and is slightly less than $2 \times N_{BM}$, where N_{BM} refers to the BM group delay expressed in number of cycles. Despite significant variability, the N_{SFOAE} values predicted from individual RNS (the dots in Fig. 3C) follow this general trend. In a manner consistent with the overestimation of the BM phase slope in Fig. 1, the predicted N_{SFOAE} tends to be above measurements in gerbils by a factor 2 to 2.3.

The correlation between N_{SFOAE} and tuning sharpness is evaluated by plotting N_{SFOAE} as a function of Q_{ERB}. As the frequency is swept, Fig. 3D shows that the variations in N_{SFOAE} and Q_{ERB} are correlated, in both model predictions (at least for frequencies up to 30 kHz) and experiments in gerbils: the broader tuning observed at more apical locations is generally associated with lower normalized group delays. However, as observed in Fig. 3C, the predicted N_{SFOAE} values are significantly above the measured N_{SFOAE} values.

Note that throughout the paper, Q_{ERB} and N_{BM} are calculated using the smooth model. This approach cannot be directly followed in an experiment since roughness cannot be eliminated. However, we show in Appendix 3 that the

model with roughness yields values of Q_{ERB} and N_{BM} that are nearly identical to those obtained with the smooth model if filtering is applied to eliminate the secondary reflections.

Effect of Changes in Parameters or Stimulus Level on BM and SFOAE Responses

Figure 4 shows the effect of varying model parameters or stimulus level on the amplitude and phase of the BM response and of SFOAEs predicted for one single RNS. In all cases, the changes in model parameters or increase in the SPL cause (1) a reduction in the amplitude of the BM velocity response (Fig. 4 A–D), (2) a broadening of the BM velocity response (Fig. 4 E–H), and (3) a reduction in the SFOAE amplitude (Fig. 4 I–L). In cases of reduced HB current, increased TMLC, and increased SPL, these changes in amplitudes and tuning sharpness are associated with decreases in the peak frequency (Fig. 4 A, B, and D) and in the slopes of the phase

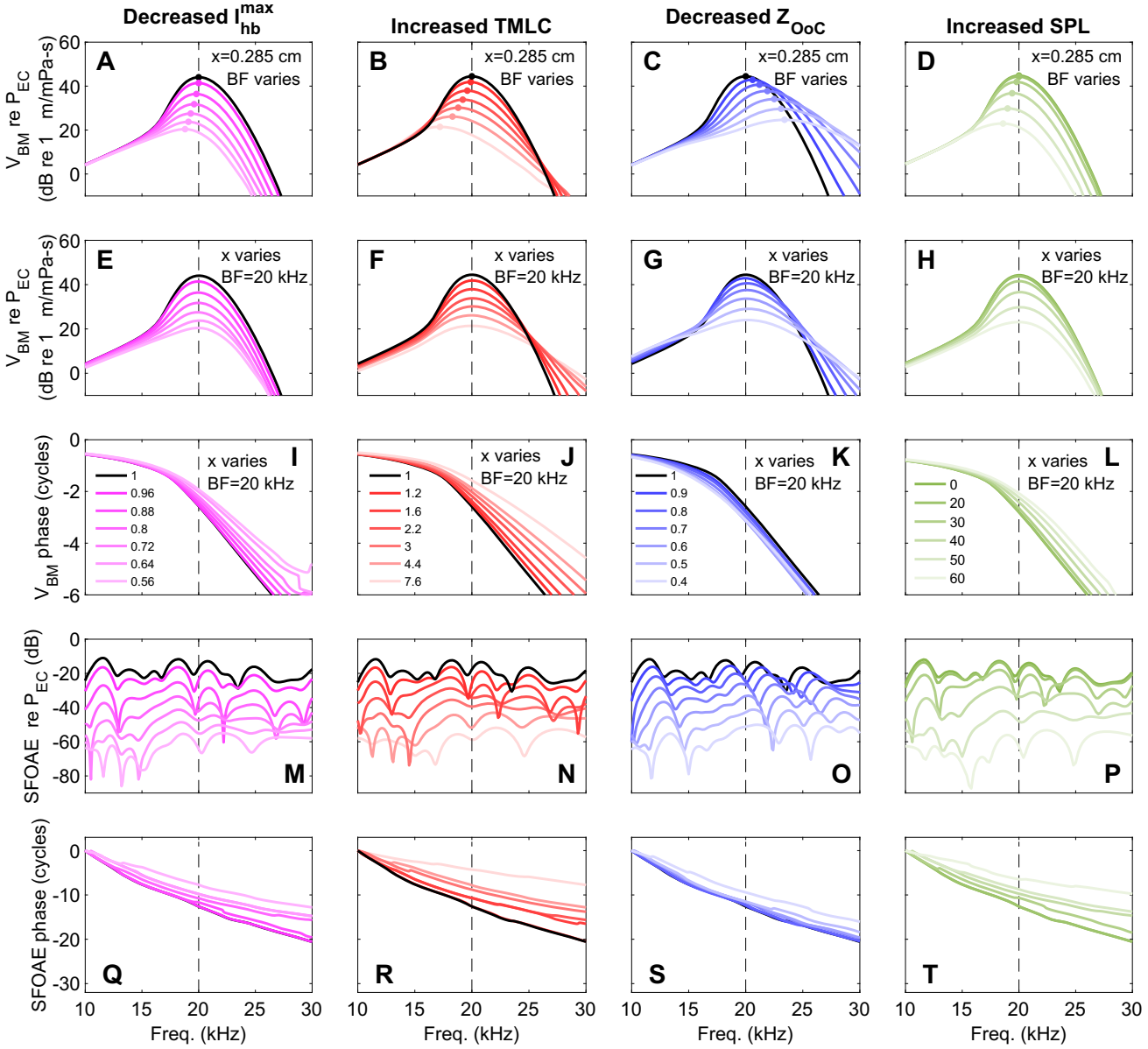

Fig. 4 Effect of varying model parameters and the level of the stimulus on BM velocity and SFOAEs. Amplitude (**A**–**H**) and phase (**I**–**L**) of the BM velocity relative to the EC pressure. In **A**–**D**, the longitudinal location is fixed to the 20 kHz CP of the smooth baseline model; in this case, the BF varies as the parameter varies. In **E**–**L**, the longitudinal location is varied so that all curves peak at the same frequency of 20 kHz. Keeping the peak frequency invariant facilitates the comparison of the shape of the amplitude response and of the slope of the phase response. **M**–**T** SFOAE amplitude relative to the EC pressure (**M**–**P**) and SFOAE phase (**Q**–**T**) relative to the SFOAE phase at 10 kHz. The SFOAE results are the filtered SFOAE with the first reflection only for a single RNS. In the last column, the sound pressure level was varied from 0 to 60 dB SPL

of both the BM velocity (Fig. 4 I, J, and K) and SFOAE (Fig. 4 Q, R, and T), implying that the group delays are significantly reduced. However, in the case of varied OoC parameters, the peak frequency increases (Fig. 4C) and the slope of the phase responses is not affected as significantly as in the other cases (Fig. 4 K and S).

Figure 5 shows Q_{ERB} and N_{SFOAE} plotted as a function of the scaling factor used to control each parameter variation. All parameters were varied such that the range of Q_{ERB} is roughly similar for all parameter variations (from 6.6 in the baseline model to 3, as seen in the 1st row of Fig. 5). However, N_{SFOAE} is observed to vary much more significantly in the cases of the decreased HB current, increased TMLC, and increased stimulus level than in the case of varied OoC parameters (2nd row of Fig. 5). Overall, a monotonic trend is observed between the scaling factor and N_{SFOAE}. N_{SFOAE} is close to $2 \times N_{BM}$ in the baseline case. In all cases, as the parameter variations cause a reduction in Q_{ERB}, the loess fit of N_{SFOAE} progressively deviates slightly from the $2 \times N_{BM}$ curve.

Relation Between SFOAE Delays and Cochlear Tuning

Figure 6 shows how the variations in model parameters or in the SPL of the stimulus affect the relation between N_{SFOAE} and Q_{ERB}. For all parameter variations, N_{SFOAE} is positively correlated with Q_{ERB} (Fig. 6A, solid lines). In the case of increased TMLC, N_{SFOAE} is nearly proportional to Q_{ERB} as it follows the black dashed line. The curve N_{SFOAE} *vs.* Q_{ERB} deviates from a proportional relation in the three other cases. The curve N_{SFOAE} *vs.* Q_{ERB} is below the proportional line in the case of decreased MET current and increased SPL; the opposite trend is observed in the case of decreased OoC impedance. In all cases, the curves for N_{SFOAE} vs. Q_{ERB} are slightly below the corresponding $2 \times N_{BM}$ vs. Q_{ERB} curve (dotted lines).

The link between N_{SFOAE} and Q_{ERB} can also be examined by calculating the SFOAE tuning ratio, defined as $\alpha_{SFOAE} = Q_{ERB}/N_{SFOAE}$ [5]. α_{SFOAE} is nearly invariant in the case of increased TMLC. Decreasing the MET current or increasing the SPL causes moderate, non-monotonic variations of α_{SFOAE}. However, varying the OoC parameters causes a significant decrease in α_{SFOAE}. The variations in α_{SFOAE} are the consequence of two factors, which can be understood by writing α_{SFOAE} as the product of two terms:

$$\alpha_{SFOAE} = \alpha_{BM} \times \frac{2N_{BM}}{N_{SFOAE}} \tag{7}$$

where $\alpha_{BM} = Q_{ERB}/(2N_{BM})$ is the BM tuning ratio, which is plotted in thin dotted lines in Fig. 6B. In this analysis, N_{BM} corresponds to the BM group delay evaluated at the BP of the model for the chosen values of the parameters or stimulus level. α_{BM} varies significantly in the case of varied OoC parameters, which can be interpreted as a change in the type and/or order of the BM filters as the parameter varies. More-

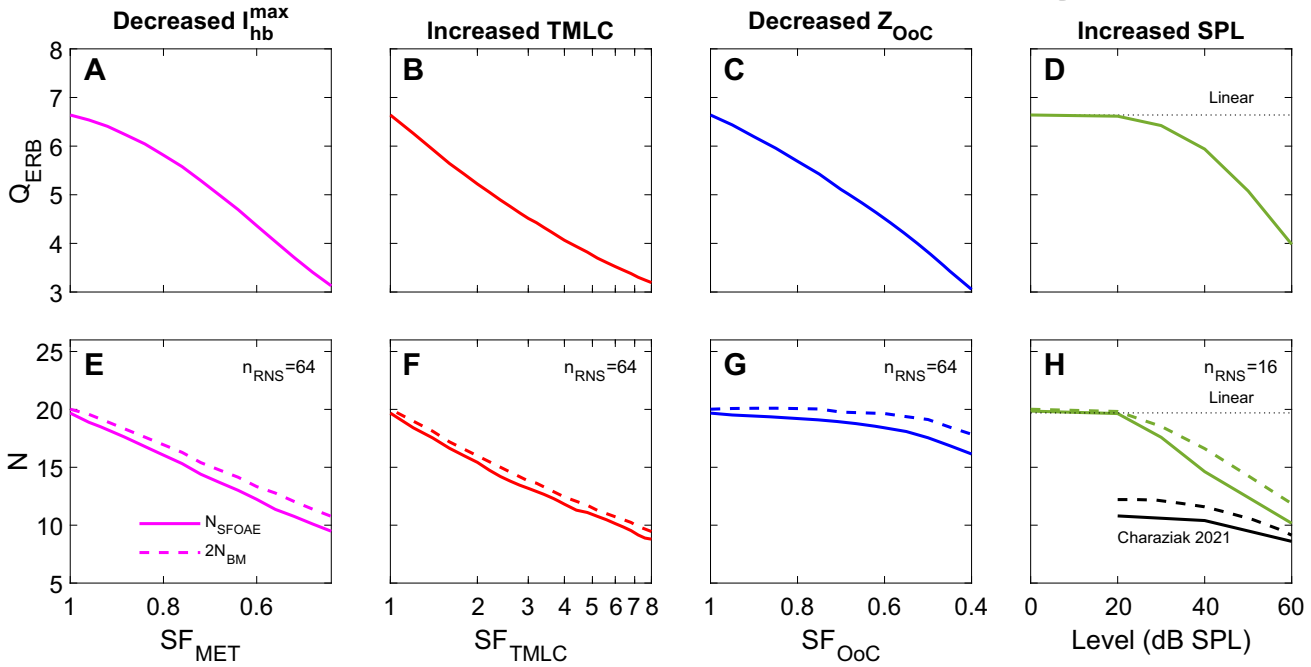

Fig. 5 Effect of parameter variations and changes in stimulus level on BM tuning sharpness and phase-gradient delay. **A–D** Q_{ERB} of the BM velocity, evaluated at the 20 kHz BP. **E–H** N_{SFOAE} is plotted at 20 kHz. The loess fit of the N_{SFOAE} predicted by the model with roughness for multiple RNS values is compared to $2 \times N_{BM}$ (obtained with the smooth model)

over, in all cases, the ratio N_{SFOAE}/N_{BM}, which is plotted in Fig. 6C, also varies; for all parameter variations, a reduction of Q_{ERB} is associated with a nearly monotonic decrease in this ratio. When Q_{ERB} is large, this ratio approaches 2; as Q_{ERB} decreases, the ratio drops progressively to around 1.7 to 1.85 depending on the parameter variation.

How Do N_{SFOAE} Simulations Predict Q_{ERB}?

The fact that N_{SFOAE} is approximately proportional to Q_{ERB} (or equivalently that the SFOAE tuning ratio is nearly invariant) suggests that measuring N_{SFOAE} can directly be used to estimate Q_{ERB}. This is what was used by Shera et al. [27] to estimate cochlear tuning in humans at the population level. We evaluate in Fig. 7 how simulations of N_{SFOAE} can be used to estimate the Q_{ERB} of the model, both for the case of

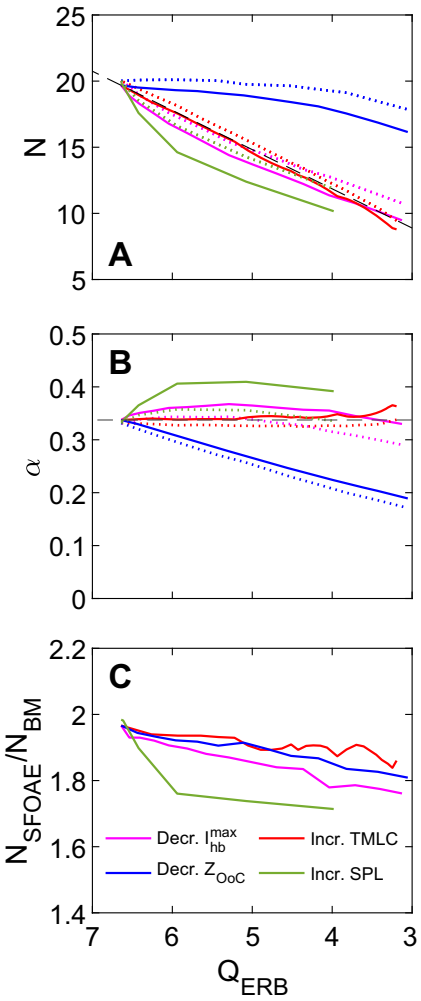

Fig. 6 Link between SFOAE delays and cochlear tuning. **A** N_{SFOAE} (thick solid lines) and $2N_{BM}$ (thin dotted lines) plotted as a function of Q_{ERB}. **B** BM (thin dotted lines) and SFOAE (thick solid lines) tuning ratios, α_{BM} and α_{SFOAE}. The black thin dashed lines in **A** and **B** correspond to a constant tuning ratio of 0.3374, which is the tuning ratio of the baseline model. **C** Ratio of N_{SFOAE} to N_{BM}

the N_{SFOAE} predicted for a single RNS, and for the loess fit of multiple RNSs. Even in the case of a computer simulation which is not affected by noise and measurement errors, the ability of using a single N_{SFOAE} measurement to estimate Q_{ERB} is more challenging due to the inherent variability of N_{SFOAE} linked to the generation mechanism of SFOAE.

Figure 7A illustrates the process used to estimate Q_{ERB} for a single simulation. The group delay predicted for a single RNS value at an MET scaling factor of 0.80 is shown in a thin magenta line, along with the peak-picked values indicated using dots. We chose to quantify the error in the N_{SFOAE}-based estimate of Q_{ERB} at a single frequency of 20 kHz which is the midpoint of the frequency range of 10 to 30 kHz used for these simulations. To reliably estimate N_{SFOAE} at 20 kHz for that single simulation, the peak-picked values of N_{SFOAE} were fitted using a linear function of frequency:

$$N^{fit}_{SFOAE}(f) = \beta_0 + \beta_1 f \tag{8}$$

The least square fit, $N^{fit}_{SFOAE}(f)$, plotted in a thick magenta line, captures the general trend seen in the simulation for the chosen RNS value. Furthermore, this fit is close, but not identical, to the loess fit of the 64 RNS for the SF_{MET} considered in this simulation.

$N^{fit}_{SFOAE}(f = 20\text{kHz})$ is used to estimate Q_{ERB} at 20 kHz by using the equation:

$$\tilde{Q}_{ERB}(f) = \frac{N^{fit}_{SFOAE}(f)}{\alpha_{SFOAE}(f, SF_{MET} = 1)} \tag{9}$$

where $\alpha_{SFOAE}(f, SF_{MET} = 1)$ is the SFOAE tuning ratio of the baseline model. The process was repeated for all SF_{MET} values. For the RNS value used in Fig. 7B, the estimate of Q_{ERB} based on Eq. 9 is observed to approximately follow the curve $Q_{ERB}(SF_{MET})$ directly calculated from simulations of the BM response.

To quantify the precision and accuracy of this method, the percent relative error in the estimate of Q_{ERB} was calculated as follows:

$$\mathcal{E}_{Q_{ERB}} = 100 \times \frac{\tilde{Q}_{ERB} - Q_{ERB}}{Q_{ERB}} \tag{10}$$

where Q_{ERB} refers to the true value of Q_{ERB}, (i.e., the value directly obtained from the simulation of the BM response) and $\tilde{Q}_{ERB}$ refers to the value obtained from N_{SFOAE}. $\mathcal{E}_{Q_{ERB}}$ is plotted as a function of the true Q_{ERB} in Fig. 7 C–F for the variations in model parameters or stimulus levels. The dots show the error for individual RNS values. In the case of decreased SF_{MET}, increased SF_{TMLC}, and increased SPL, the error is relatively small (less than 20% for all individual RNS). The mean error (shown in a solid line) is negative in the case of decreased SF_{MET} and increased SPL, which

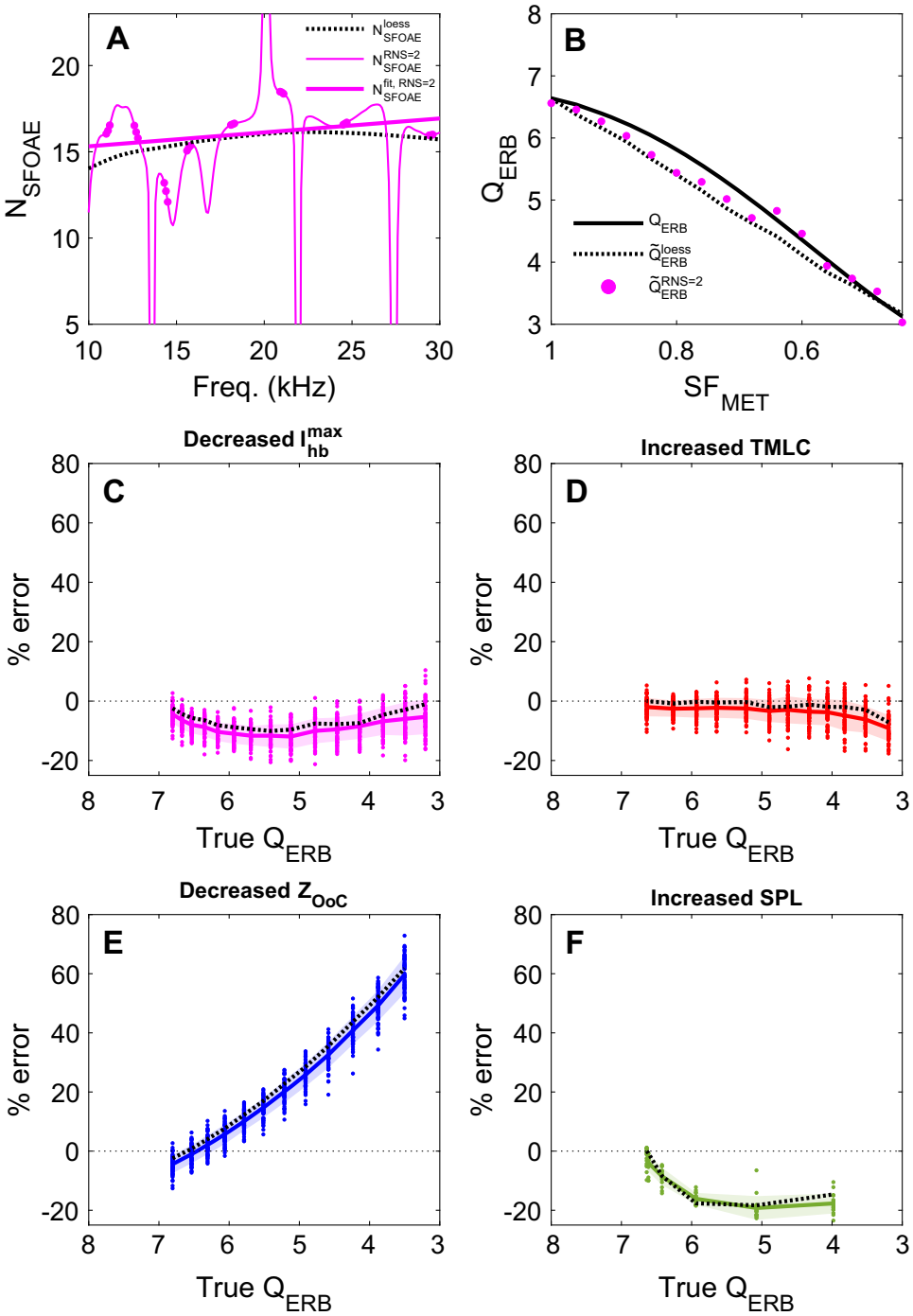

Fig. 7 Estimation of Q_{ERB} based on N_{SFOAE} simulations. **A** Comparison of the N_{SFOAE} predicted for a single simulation (RNS=2) for $SF_{MET} = 0.8$ (thin magenta line) to the least squares fit using Eq. 8 (thick magenta line). The trend line obtained using the loess fit of 64 RNS for $SF_{MET} = 0.8$ is shown in a thick black dotted line for reference. **B** Comparison of $\tilde{Q}_{ERB}$ calculated from the fit of SFOAE delay at 20 kHz shown in **A** using Eq. 9 to the true value directly calculated from the predicted BM response, Q_{ERB}. **C**–**F** The percent relative error between $\tilde{Q}_{ERB}$ and Q_{ERB} is plotted as a function of Q_{ERB} in the case of decreased I_{hb}^{max} (**C**), increased TMLC (**D**), decreased Z_{OoC} (**E**), and increased SPL (**F**). The dots correspond to individual RNS cases; the solid lines and the shaded area represent the mean and ± one standard deviation, respectively. The black dotted line in **C**–**F** is the error for the $\tilde{Q}_{ERB}$ estimated based on the loess fit of all RNS

is due to the fact that, in these cases, the N_{SFOAE} curve is above the constant α_{SFOAE} curve in Fig. 6A. The mean error is very close to 0 in the varied TMLC case and remains less than 10% in the decreased I_{hb}^{max} case. However, the method overestimates Q_{ERB} by large errors of up to 70% in the case of increased Z_{OoC}, which is due to the deviation of N_{SFOAE} from the constant α_{SFOAE} case in Fig. 6A. These results show that N_{SFOAE} predicted for a single ear allows for an estimate of Q_{ERB} of reasonable accuracy (errors of up to 20%) for the varied MET, TMLC, and level cases. However, for the case of varied Z_{OoC} that affects significantly the shape of the BM response but not the SFOAE delays, the method is unable to estimate Q_{ERB} reliably.

The mean error of the $\tilde{Q}_{ERB}$ predicted for all RNS tends to be slightly negative in the case of decreased I_{hb}^{max}, increased TMLC, and increased SPL. This error is linked to the fact that the SFOAE tuning ratio drops slightly below the value of the baseline model in Fig. 6B. Another approach for multiple

RNS is to use the loess fit to directly obtain N_{SFOAE}^{loess} at 20 kHz, before using this value in Eq. 9 to calculate an estimate of Q_{ERB}. The estimate based on the loess fit, shown in a black dotted line in Fig. 7 C–F, is observed to be nearly identical to the mean error shown in the solid line.

Discussion

This work utilizes a physiologically motivated model of the gerbil cochlea to investigate how changes in cochlear tuning affect SFOAE phase-gradient delays. After calibration, the baseline model predicts a similar BM amplitude response as in in vivo measurements in gerbils, with similar Q_{ERB} values (Fig. 1). However, the group delays of the BM response and of SFOAEs are higher than in experiments by a factor of around two. The slope of the N_{SFOAE} vs. frequency curve is predicted to be shallower than in experiments. Computational models of the cochlea that rely on coherent reflection have been previously used to simulate SFOAEs and study their generation mechanisms and key characteristics [17, 18, 28, 29]. While these previous models have not been used to systematically study the link between the sharpness of cochlear tuning and SFOAE delays, they often predict higher group delays than in experiments (e.g., [28]). More phenomenological models can be more easily tuned to predict more realistic SFOAE group delays [30].

Another way to evaluate the SFOAE predicted by the model is by examining the ratio of SFOAE group delays to BM group delays. The baseline model predicts that the ratio of SFOAE group delay to BM group delay is near two (1.95), which is a bit higher than has been observed in experiments: N_{SFOAE} has been found to vary between $1.2\times$ and $1.8\times$ N_{BM}, depending on the species, including 1.6 in gerbils [16]. In the current model, SFOAEs originate primarily from the peak of the traveling wave. Because this model has purely local OHC feedback, the delays of forward and reverse waves are nearly identical, such that the SFOAE delay is about twice the BM group delay in the case of a sharply tuned model. The finite element model from Motallebzadeh and Puria [28], which includes non-local OHC feedback due to the cytoarchitecture of the organ of Corti, predicts a much lower value for N_{SFOAE}/N_{BM} of about 0.6. Shera and Altoe [30] demonstrated that varying the locality of the OHC feedback allows N_{SFOAE}/N_{BM} to vary significantly. They concluded that the values reported in experiments for N_{SFOAE}/N_{BM} suggest that the OHC feedback is primarily local; however, introducing a small amount of non-locality in our model by accounting for the longitudinal tilt of OHCs might be needed to lower the predictions of our model for N_{SFOAE}/N_{BM} to values closer to experiments.

The limitations in the accuracy of the N_{SFOAE} predictions of the baseline model should not deter from using the model in improving understanding of the correlations between tuning sharpness and SFOAE phase-gradient delays. In order to limit the computational cost, the study of the effect of model parameter variations on Q_{ERB} and N_{SFOAE} was conducted using a linear frequency-domain implementation of the model, such that the results obtained here only directly apply to SFOAEs measured in response to the stimulus of level up to about 20 dB SPL. However, the findings are expected to be qualitatively similar for higher sound pressure levels. All model parameter variations considered in this article cause concurrent changes in Q_{ERB} and N_{SFOAE}, i.e., reductions in Q_{ERB} are associated with lower N_{SFOAE}. N_{SFOAE} and Q_{ERB} are nearly proportional to each other in the case of increased TM longitudinal coupling; the relationship between N_{SFOAE} and Q_{ERB} is close to being proportional in the decreased HB current case but not in the varied OoC impedance case. This lack of proportionality in the varied OoC impedance case arises because the BM tuning ratio is significantly affected by the parameter variations. The filter theory used by Shera [5] to interpret the relationship between group delay and tuning sharpness relies on the assumption that the overall transfer function between input (EC pressure) and output (BM displacement) can be represented as a filter of fixed type (for example, a gammatone filter) and order. The type and order of the BM filters are not directly available in the model as these depend on the hydrodynamics of the fluid, the micromechanics of the organ of Corti, and the electromechanical feedback from OHCs. Nevertheless, it may be possible to fit (or approximate) the transfer function of the BM response using specific filters. As discussed by Shera, for a given filter of fixed order, bandwidth and group delay are simply related: for example, for a gammatone filter of order n, the normalized group delay N is related to the quality factor Q_{3dB} by the equation: $N = n\sqrt{2^{1/n}-1}Q_{3dB}/\pi$ [31]. The lack of invariance of the BM tuning ratio in the varied OoC impedance case suggests that the effect of this parameter's variation cannot be captured by a simple change in the parameters of fixed type and order of the BM filter, but that the type and/or order of the filter changes when the parameter is varied. The possibility that the tuning ratio may change significantly needs to be kept in mind when SFOAE phase-gradient delays are used to estimate cochlear tuning in multiple species, or in animals with altered properties (such as transgenic mice with altered TM protein expressions [26]).

In addition to this change in the tuning ratio, all parameter variations affect the ratio of N_{SFOAE} to N_{BM}: in all cases, the broadening of cochlear tuning is correlated with a moderate reduction in N_{SFOAE}/N_{BM}. With broader tuning, the SFOAE generation region becomes broader and the size of contributions from locations basal to the peak increases relative to contributions from the peak. This shift in the SFOAE generation is the likely source of the reduction of the N_{SFOAE} to N_{BM} ratio.

The effect of increasing sound pressure level is predicted to be quite similar to the effect of directly reducing the MET current. The nonlinear model predicts that increases in SPL cause broadening of BM tuning, and decreases in BM and SFOAE delays (of the 1st reflection component), as observed in experiments. This relation between Q_{ERB} and N_{BM} when SPL is increased is similar, but not identical, to the trend observed when the MET current is reduced. As observed in the experimental data from Charaziak and Shera [16], the BM tuning ratio is nearly level-independent when SPL is increased, such that N_{BM} is predicted to be nearly proportional to Q_{ERB}. The ratio of N_{SFOAE} to N_{BM} is predicted to depend weakly on SPL. Although Charaziak and Shera observed that the ratio of N_{SFOAE} of the 1st reflection component to N_{BM} is nearly constant when stimulus level is varied, our model predicts that the broadening of cochlear tuning at higher SPL is associated with somewhat lower N_{SFOAE} to N_{BM} ratios (Fig. 6C).

The use of our model allows us to evaluate how SFOAE delays may be used to estimate the sharpness of cochlear tuning. We focus not only on group-level predictions (i.e., for multiple RNS values in Fig. 7), as done previously in experiments in different species, but also on predictions for a single RNS (which represent data from a single ear). The method assumes that Q_{ERB} and N_{SFOAE} are proportional to each other. When applied at the population level (i.e., when estimations for multiple RNS values are averaged, either based on the loess fitting or by taking the median of individual Q_{ERB} estimates), the only source of error is the lack of exact proportionality between Q_{ERB} and N_{SFOAE}. Because a proportional relation between Q_{ERB} and N_{SFOAE} is a decent approximation in the case of varied MET current and TMLC, the population level estimates of Q_{ERB} are within a few percents of the directly predicted values. A somewhat larger error is observed for the case of varied stimulus level due to the larger deviation from proportionality. However, when the Z_{OoC} varied, the error can reach very large values due to the lack of proportionality between Q_{ERB} and N_{SFOAE}, making the method useless.

Estimation of Q_{ERB} from a single simulation (or experiment) is more challenging due to variability of the N_{SFOAE} *vs.* frequency curve for a single RNS. It is essential to extract a meaningful trend for the curve of N_{SFOAE} *vs.* frequency, which is representative of cochlear tuning rather than of the inherent variability of the coherent reflection mechanism. To eliminate the variability, the values of N_{SFOAE} were fitted using a simple linear function of frequency; other functional dependencies for the curve $N_{SFOAE}(f)$ were considered (not shown), but this did not significantly affect the results. The error between the Q_{ERB} estimated using a single simulation and the true Q_{ERB} is somewhat larger than the error observed at the population level, but remains reasonable (i.e., less than 20%) in the decreased MET current and increased TMLC cases. For the single RNS case, this error arises from two sources: 1) the error in the estimation of the $N_{SFOAE}(f)$ trendline and 2) error in the relation between N_{SFOAE} and Q_{ERB} (i.e., N_{SFOAE} is not exactly proportional to Q_{ERB}).

In conclusion, the use of a computational model allows us to study the link between the sharpness of cochlear tuning and SFOAE delays in a well-controlled environment. We found that most model parameter variations cause nearly proportional variations in Q_{ERB} and N_{SFOAE}, making it possible to estimate Q_{ERB} from N_{SFOAE}. However, the numerical results highlight the fact that it may be possible for changes in model parameters to cause non-proportional changes in Q_{ERB} and N_{SFOAE}.

Appendix 1: Table of Model Parameters

Table 1 Updated mechanical and electrical parameters for cochlear model, where x is the longitudinal position in cm

Param.	Description	Value in Ref. [7]	Value in present study
K_{tms}	TM shear stiffness (per unit length)	$2.772 \times 10^5 \cdot e^{-6.422279x-1.319184x^2}$ N/m$_2$	$2.772 \times 10^5 \cdot e^{-7.5425x}$ N/m$_2$
C_m	Basolateral capacitance (per OHC)	$17.45x$ pF	$1.6933 \cdot e^{4.08x}$ pF
G_m	Basolateral conductance (per OHC)	$192 - 148.9x$ nS	$55 \cdot e^{2x}$ nS
G_{hb}^{max}	Saturating HB MET conductance (per HB)	Interpolated from	Interpolated from
		97.6 nS at x=0 cm	109.5 nS at x=0 cm
		94.3 nS at x=0.13 cm	87.2 nS at x=0.13 cm
		74.9 nS at x=0.224 cm	70.9 nS at x=0.224 cm
		56.2 nS at x=0.32 cm	56.9 nS at x=0.32 cm
		38.4 nS at x=0.44 cm	42.5 nS at x=0.44 cm
		18.8 nS at x=0.67 cm	23.0 nS at x=0.67 cm
		1.97 nS at x=1.12 cm	17.4 nS at x=0.75 cm
			2.0 nS at x=1.12 cm

The model assumes 1000 sections per cm, each with 3 OHCs

Appendix 2: Comparison of Model with Reduced SF_{MET} to Experiments

The tuning and delays of a model with reduced MET current ($SF_{\mathrm{MET}} = 0.88$) are compared to experiments and to the baseline model ($SF_{\mathrm{MET}} = 1$) in Fig. 8. The first row of Fig. 8 shows a reduction in the sensitivity of the BM responses for the model with $SF_{\mathrm{MET}} = 0.88$. The second row of Fig. 8 shows reduced Q_{ERB} (Fig. 8D), N_{BM}, and N_{SFOAE} (Fig. 8E) for the model with $SF_{\mathrm{MET}} = 0.88$ in comparison to the baseline. Even though the model with reduced MET current predicts a BM amplitude response that nearly matches (at the 26 kHz and 35.5 kHz CPs) or even below (at the 18 kHz CP) the experimental curves, the BM and SFOAE delays of this model remain significantly above the experimental values. The link between tuning sharpness and delays, upon which our analysis rests, is unaffected by the exact values of Q_{ERB}, N_{BM}, and N_{SFOAE} of the baseline model.

Appendix 3: Calculation of Q_{ERB} and N_{BM} Using Filtered Response of Model with Roughness

Introducing roughness affects the frequency response of the BM to a pure tone (Fig. 9 A and C): with roughness, the amplitude and normalized group delay curve have a fine structure. If the Q_{ERB} and N_{BM} at BF are directly calculated from the response of the rough models, there is variability in the calculated values (Fig. 9 B and D). While the median value of the N_{BM} calculated for all RNS is nearly identical to the N_{BM} calculated for the smooth model, the median Q_{ERB} is significantly above the Q_{ERB} of the smooth model. To obtain more reliable estimates of Q_{ERB} and N_{BM}, we applied filtering on the IFFT of the response of the model with roughness (Fig. 9E) to eliminate the lobes of longer delays due to secondary reflections. The FFT of this filtered IFFT looks nearly identical to the smooth model response near BF and lacks any fine structure in this region (Fig. 9 A and C). As a result, the Q_{ERB} and N_{ERB} values are nearly independent of the

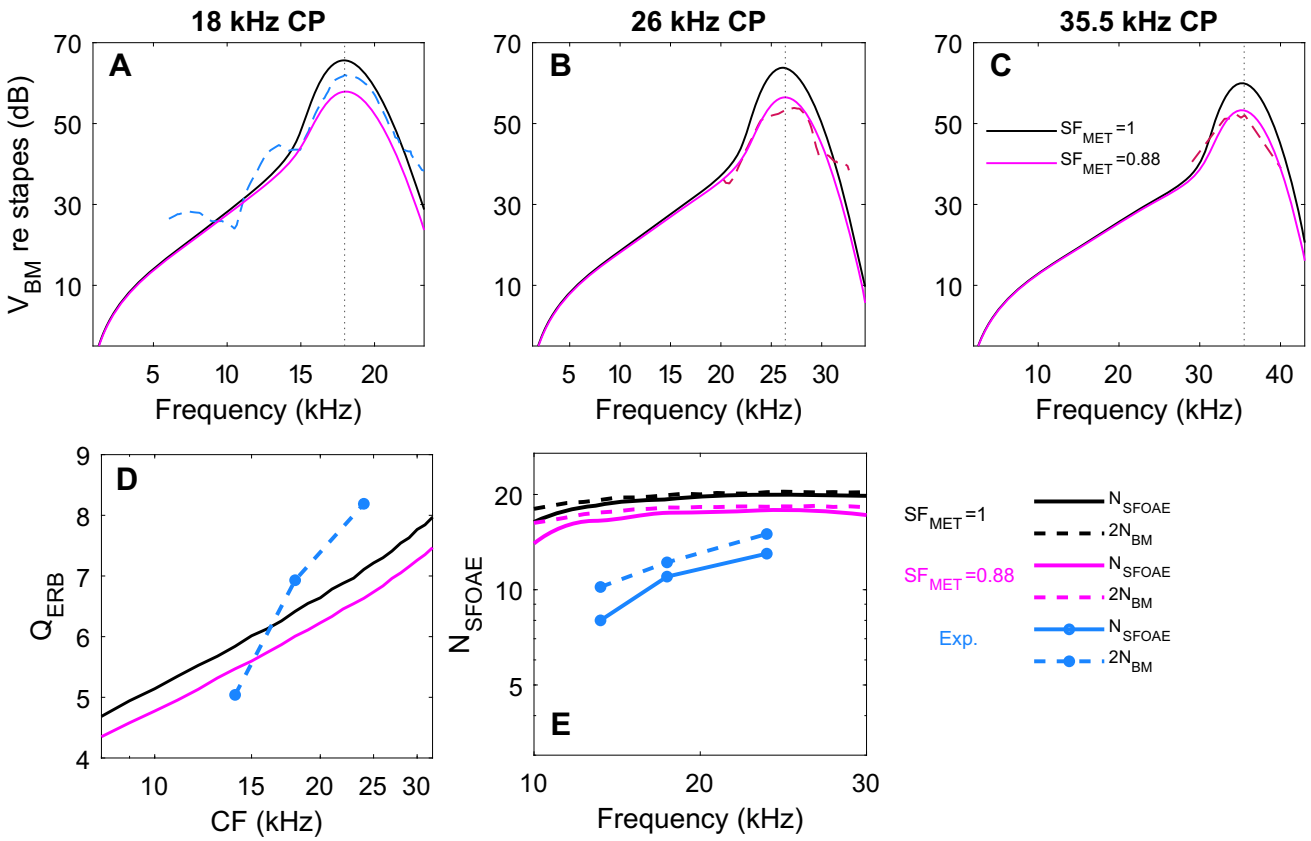

Fig. 8 Effect of reduced SF_{MET} on tuning and delays. **A**–**C** The amplitude of BM velocity relative to stapes velocity. **D** and **E** Q_{ERB} of the BM velocity and normalized group delays, respectively. Experimental responses are at 20 dB SPL in **A** and at 30 dB SPL in **B** and **C** and correspond to the same experiments in Fig. 1 of the main text. Model responses are of the active linear model using $SF_{\mathrm{MET}} = 1$ (baseline model) and $SF_{\mathrm{MET}} = 0.88$. Simulations in **E** and **J** are compared to experimental measurements in gerbils from Charaziak and Shera [16]

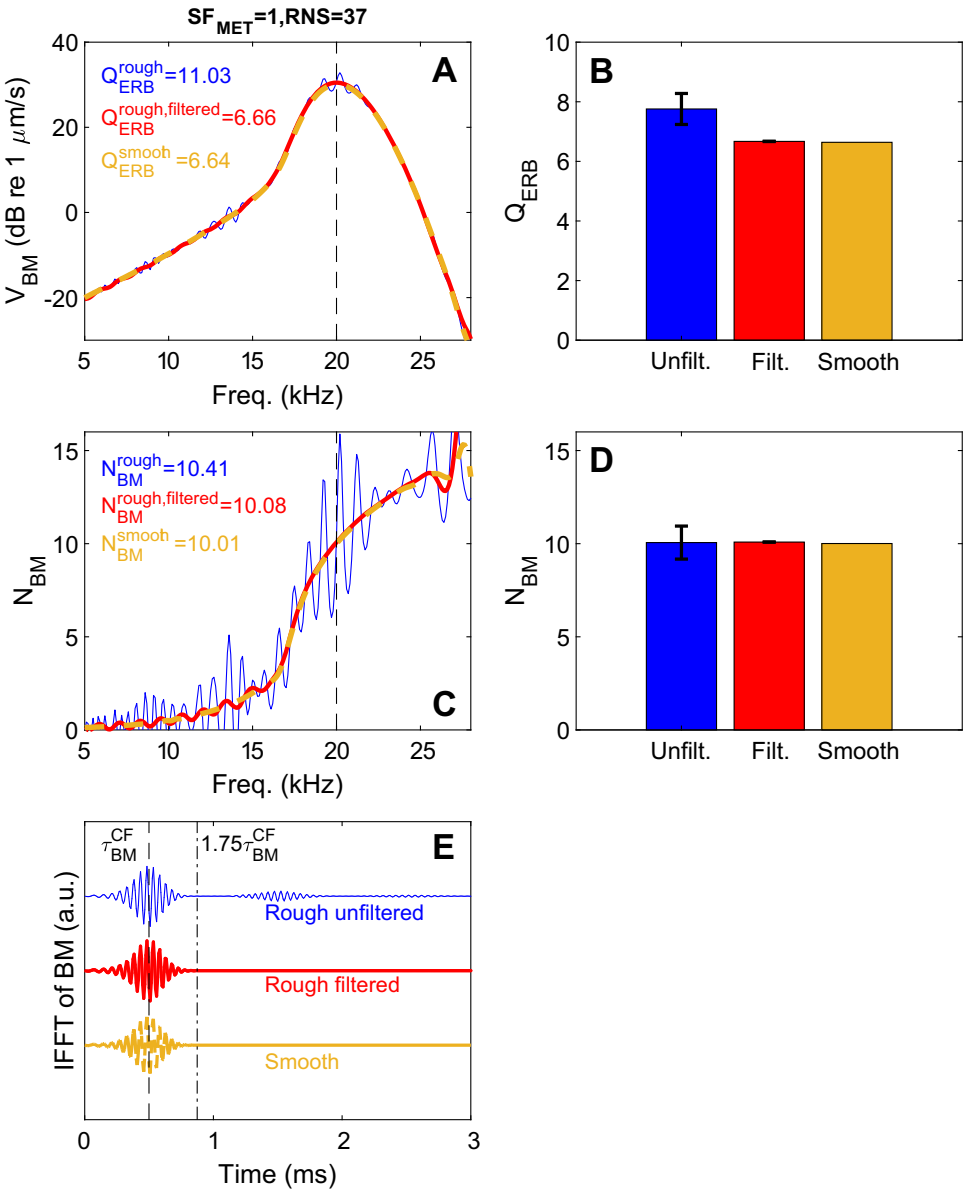

Fig. 9 Comparison of Q_{ERB} and N_{BM} calculation using rough unfiltered, rough filtered, and smooth BM responses. **A**, **C**, and **E** The unfiltered, filtered, and smooth BM response amplitude (**A**), normalized group delay (**C**), and waveform (**E**) for one RNS. **B** and **D** Median (bar height) and IQR (error bar) of Q_{ERB} (**B**) and N_{BM} (**D**) calculated with unfiltered and filtered BM response, using 64 simulations with different RNS values and $SF_{\mathrm{MET}} = 1$. The smooth value is also shown for reference in **B** and **D**

RNS and are nearly identical to the values obtained with the smooth model (Fig. 9 B and D).

Acknowledgements No AI was used for either manuscript preparation or research purposes.

Author Contribution Conceptualization: JM. Methodology: YX, GS, JM. Investigation: YX, GS, JM. Visualization: YX, GS, JM. Funding acquisition: JM. Project administration: JM. Supervision: SM. Writing—original draft: YX, JM. Writing—review and editing: JM and GS.

Funding This research was funded by NIH Grant R01 DC016114.

Data Availability Data sets generated during the current study are available from the corresponding author on reasonable request.

Code Availability Codes written during the current study are available from the corresponding author on reasonable request

Declarations

Conflict of Interest The authors declare no competing interests.

References

1. Robles L, Ruggero MA (2001) Mechanics of the mammalian cochlea. Physiol Rev 81(3):1305–1352
2. Kemp DT (2002) Otoacoustic emissions, their origin in cochlear function, and use. Br Med Bull 63(1):223–241

3. Zweig G, Shera CA (1995) The origin of periodicity in the spectrum of evoked otoacoustic emissions. The journal of the acoustical society of America. 98(4):2018–2047
4. Shera CA, Guinan JJ Jr (1999) Evoked otoacoustic emissions arise by two fundamentally different mechanisms: a taxonomy for mammalian OAES. The journal of the acoustical society of America. 105(2):782–798
5. Shera CA, Guinan JJ, Oxenham AJ (2010) Otoacoustic estimation of cochlear tuning: validation in the chinchilla. J Assoc Res Otolaryngol 11(3):343–365
6. Bowling T, Wen H, Meenderink SW, Dong W, Meaud J (2021) Intracochlear distortion products are broadly generated by outer hair cells but their contributions to otoacoustic emissions are spatially restricted. Sci Rep 11(1):1–14
7. Samaras G, Wen H, Meaud J (2023) Broad nonlinearity in reticular lamina vibrations requires compliant organ of Corti structures. Biophys J 122(5):880–891
8. Ramamoorthy S, Deo NV, Grosh K (2007) A mechano-electro-acoustical model for the cochlea: response to acoustic stimuli. The journal of the acoustical society of America. 121(5):2758–2773
9. Meaud J, Grosh K (2010) The effect of tectorial membrane and basilar membrane longitudinal coupling in cochlear mechanics. The journal of the acoustical society of America. 127(3):1411–1421
10. He W, Burwood G, Porsov EV, Fridberger A, Nuttall AL, Ren T (2022) The reticular lamina and basilar membrane vibrations in the transverse direction in the basal turn of the living gerbil cochlea. Sci Rep 12(1):19810
11. He W, Kemp D, Ren T (2018) Timing of the reticular lamina and basilar membrane vibration in living gerbil cochleae. Elife. 7:37625
12. Overstreet EH, Temchin AN, Ruggero MA (2002) Basilar membrane vibrations near the round window of the gerbil cochlea. J Assoc Res Otolaryngol 3:351–361
13. Cho NH, Puria S (2022) Cochlear motion across the reticular lamina implies that it is not a stiff plate. Sci Rep 12(1):18715
14. Shera CA, Guinan JJ Jr (2003) Stimulus-frequency-emission group delay: a test of coherent reflection filtering and a window on cochlear tuning. The journal of the acoustical society of America. 113(5):2762–2772
15. Shera CA (2001) Intensity-invariance of fine time structure in basilar-membrane click responses: implications for cochlear mechanics. The journal of the acoustical society of America. 110(1):332–348
16. Charaziak KK, Shera CA (2021) Reflection-source emissions evoked with clicks and frequency sweeps: comparisons across levels. J Assoc Res Otolaryngol 22:641–658
17. Wen H, Meaud J (2022) Link between stimulus otoacoustic emissions fine structure peaks and standing wave resonances in a cochlear model. The journal of the acoustical society of America. 151(3):1875–1894
18. Vencovskỳ V, Vetešník A, Gummer AW (2020) Nonlinear reflection as a cause of the short-latency component in stimulus-frequency otoacoustic emissions simulated by the methods of compression and suppression. The journal of the acoustical society of America. 147(6):3992–4008
19. Shera CA, Bergevin C (2012) Obtaining reliable phase-gradient delays from otoacoustic emission data. The journal of the acoustical society of America. 132(2):927–943
20. Moleti A, Longo F, Sisto R (2012) Time-frequency domain filtering of evoked otoacoustic emissions. The journal of the acoustical society of America. 132(4):2455–2467
21. Elliott SJ, Ku EM, Lineton B (2007) A state space model for cochlear mechanics. The journal of the acoustical society of America. 122(5):2759–2771
22. Meaud J, Lemons C (2015) Nonlinear response to a click in a time-domain model of the mammalian ear. The journal of the acoustical society of America. 138(1):193–207
23. Keithley EM (2020) Pathology and mechanisms of cochlear aging. J Neurosci Res 98(9):1674–1684
24. Ghaffari R, Aranyosi AJ, Richardson GP, Freeman DM (2010) Tectorial membrane travelling waves underlie abnormal hearing in Tectb mutant mice. Nat Commun 1(1):96
25. Lemons C, Sellon JB, Boatti E, Filizzola D, Freeman DM, Meaud J (2019) Anisotropic material properties of wild-type and Tectb-/- tectorial membranes. Biophys J 116(3):573–585
26. Cheatham MA (2021) Comparing spontaneous and stimulus frequency otoacoustic emissions in mice with tectorial membrane defects. Hear Res 400:108143
27. Shera CA, Guinan JJ, Oxenham AJ (2002) Revised estimates of human cochlear tuning from otoacoustic and behavioral measurements. Proc Natl Acad Sci 99(5):3318–3323
28. Motallebzadeh H, Puria S (2022) Stimulus-frequency otoacoustic emissions and middle-ear pressure gains in a finite-element mouse model. The Journal of the Acoustical Society of America. 152(5):2769–2780
29. Choi Y-S, Lee S-Y, Parham K, Neely ST, Kim DO (2008) Stimulus-frequency otoacoustic emission: measurements in humans and simulations with an active cochlear model. The Journal of the Acoustical Society of America. 123(5):2651–2669
30. Shera CA, Altoè A (2023) Otoacoustic emissions reveal the micromechanical role of organ-of-Corti cytoarchitecture in cochlear amplification. Proc Natl Acad Sci 120(41):2305921120
31. Hartmann WM (2004) Signals, sound, and sensation. Springer, New-York, USA